Statistics in Volcanology
Volume 1
February 2, 2015

High-Resolution Ground-Based Magnetic Survey of a Buried Volcano: Anomaly B, Amargosa Desert, NV

George, O., McIlrath, J., Farrell, A., Gallant, E., Kinman, S., Marshall, A., McNiff, C., Njoroge, M., Wilson, J., Connor, C. B., Connor, L. J., Kruse, S.

University of South Florida, School of Geosciences, Tampa, Florida USA

Abstract

Aeromagnetic surveys over the Amargosa Desert, Nevada, have revealed the presence of several magnetic anomalies that have been interpreted to be caused by buried volcanoes; many of these anomalies have been confirmed by drilling. We present data collected from a high-resolution, ground-based magnetic survey over Anomaly B, the largest of these anomalies, that reveal details about a buried crater and its associated lava flow, not observed in the aeromagnetic surveys. These details provide insight into the nature of the eruption and volume of this buried volcano. Results from non-linear inversion demarcate a crater with a diameter of approximately 700 m and a base approximately 150 m below the ground surface. Coupled with well log data, the inversion results suggest a total volume for the Anomaly B crater area and associated lava flows of approximately $1.0 \pm 0.4\,\mathrm{km}^3$, based on an estimated lava flow field area of $24\,\mathrm{km}^2$ and a lava thickness of 42 ± 15 m. A workflow is presented for processing such large ground-based magnetic data sets with attendant GPS data, filtering these data and constructing maps and models using the provided PERL scripts.

Keywords: ground magnetic survey, Anomaly B, buried volcano, non-linear inversion, aeromagnetic, magnetic data processing, magnetic drift correction

Correspondence:
OG: oageorge@mail.usf.edu
University of South Florida, School of Geosciences, 4202 East Fowler Ave, Tampa, FL 33620 USA.

citation:
George, O., McIlrath, J., Farrell, A., Gallant, E., Kinman, S., Marshall, A., McNiff, C., Njoroge, M., Wilson, J., Connor, C. B., Connor, L. J., Kruse, S. (2015) High-Resolution Ground-Based Magnetic Survey of a Buried Volcano: Anomaly B, Amargosa Desert, NV, *Statistics in Volcanology* 1.3 : 1 – 23. DOI: http://dx.doi.org/10.5038/2163-338X.1.3

Introduction

Statistical models of volcanic hazards rely on information about locations, ages and volumes of past events (*Bebbington & Cronin*, 2011; *Connor et al.*, 2012; *Cappello et al.*, 2012; *Bebbington*, 2013*a*; *El Difrawy et al.*, 2013; *Becerril et al.*, 2013). These hazard estimates may be biased or inaccurate if some events are not recognized, for example, if the products of a volcanic eruption are buried or eroded (*Smith & Keenan*, 2005; *Connor & Connor*, 2009; *Wetmore et al.*, 2009; *Bebbington*, 2013*b*). The potential for the products of volcanic eruptions to be buried is strongly influenced by the depositional environment in which they form (e.g., *Stamatakos et al.*, 1997). In areas with a high potential for burial, geophysical methods can play a significant role in identifying buried volcanoes and their products, and hence can improve hazard assessments (*Hill et al.*, 2002, 2009). In this paper, we use high-resolution, ground-based magnetic data to identify a magnetic anomaly, likely produced by a buried volcano and its associated lava flows. Depth of burial, lava flow volume, and crater dimensions and morphology are inferred from these data. Such inferences play an important role in volcanic hazard assessments by providing additional information about the number and location of eruptive vents and their erupted volumes and eruption dynamics. The steps used for processing and contouring the magnetic and GPS survey data are presented including the necessary PERL scripts to complete each step; this procedure could be used with other magnetic survey data. Unprocessed (raw) and processed magnetic data (more than 130,000 observations) and metadata are provided so that processing may be duplicated and to allow comparison with open-access aeromagnetic data sets collected in the same area (*USGS*, 2001).

Geologic setting

This study was conducted in the Amargosa Desert (Figure 1), south of the Nevada Test Site and south of the proposed high-level radioactive waste repository site at Yucca Mountain. Numerous volcanic hazard assessments have been conducted in the Yucca Mountain Region (YMR) (*Crowe et al.*, 1995; *Connor & Hill*, 1995; *Ho & Smith*, 1998; *Connor et al.*, 2000; *Valentine & Perry*, 2009; *Connor & Connor*, 2009; *Rechard et al.*, 2014). Volcanic hazards in the YMR are chiefly related to distributed basaltic volcanism. New episodes of volcanic activity are expected to result in the formation of new basaltic scoria cones, small lava shields and attendant lava flows. The area is characterized by a low recurrence rate of volcanism, on order of $10^{-5} - 10^{-6}$ events per year (*Connor & Hill*, 1995). Because hazard models depend on the distribution and volumes of past eruptive events (*Valentine et al.*, 2006) it is important to identify and map each of these events in as much detail as practical. Parts of the YMR are characterized by relatively high sedimentation rates, which lead to the burial of pre-Quaternary volcanoes and the partial burial of some Quaternary volcanoes (*Stamatakos et al.*, 1997). Volcanic hazard assessments can be adversely impacted, for example, if vent burial alters the apparent distribution of older vents (*Connor & Connor*, 2009). Previous studies have shown that magnetic surveys can delineate buried volcanoes in these basins (*Langenheim et al.*, 1993; *Connor et al.*, 1997, 2000), hence such data are important to use when trying to understand the volcanic history and hazards of the region.

Contoured aeromagnetic anomaly maps from airborne magnetic surveys of the Amargosa Desert show a series of anomalies (Anomalies $A - E$ in Figure 1) interpreted to be caused by buried basaltic rocks based on their high remanent magnetizations and similarities to anomalies produced by exposed basaltic lava flows, shield volcanoes and scoria cones in the region (*Bath*, 1968; *Kane & Bracken*, 1983; *Langenheim et al.*, 1991, 1993; *Grauch et al.*, 1997; *Blakely et al.*, 2000; *O'Leary et al.*, 2002). Anomalies $A - E$ are not associated with outcrops of volcanic rocks at the surface. Rather, the anomalies are of relatively short-wavelength, suggesting a shallower depth of burial when compared to the depth of older ignimbrites and Paleozoic basement rocks. Although aeromagnetic surveys are extremely useful for the identification of anomalies associated with buried basaltic rocks, ground magnetic surveys are more likely to provide details about critical volcanic features, such as the extent of lava flows (needed for volume estimates), and to distinguish near-vent facies or vent structures.

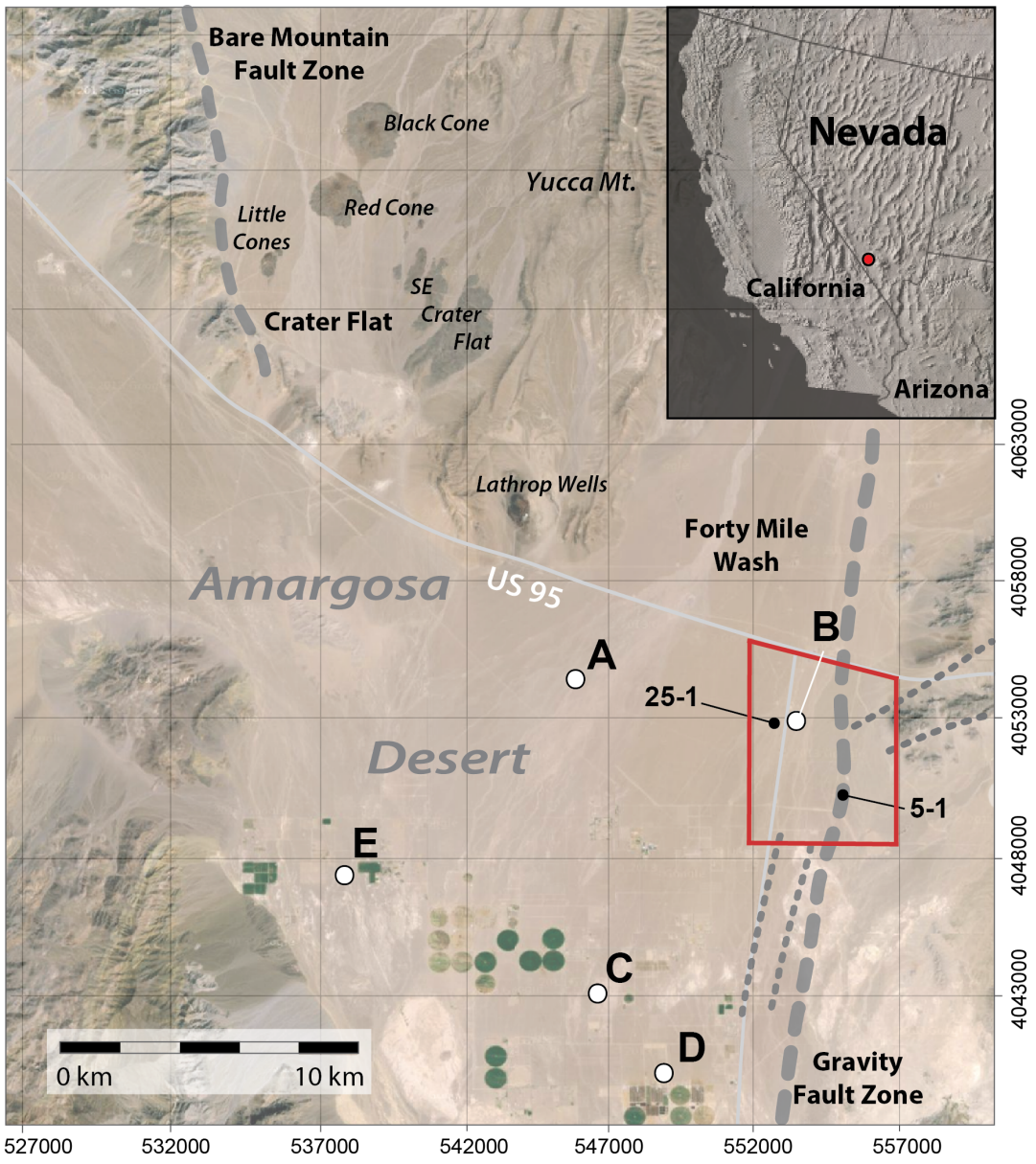

Figure 1: Survey area is located in the Amargosa Desert, near the southern tip of Nevada and immediately east of the California border, identified by the red circle on the inset map of the southwestern United States. Anomalies identified during previous aeromagnetic surveys (*Bath*, 1968; *Kane & Bracken*, 1983; *Langenheim et al.*, 1991, 1993; *Blakely et al.*, 2000; *O'Leary et al.*, 2002) are shown as white circles labeled A through E. The extent of the ground magnetic survey conducted in this study is highlighted by the red box. This anomaly has been interpreted to be caused by a buried small shield volcano and associated lava flow. Faults identified by *Carr et al.* (1995) are shown as gray dashed lines. Well logs from Felderhoff Federal drill holes 25-1 and 5-1, marked by black dots within the survey area, confirm the presence of buried basalts. Quaternary (Little Cones, Black Cone, Red Cone, Lathrop Wells) and Pliocene (SE Crater Flat) volcanoes that crop out in the area are labeled.

The relationship of buried volcanic vents to mapped geological structures that may influence vent distribution, such as basin-bounding faults, is another issue potentially resolved using ground magnetic data, provided the exact vent area can be identified and mapped (*Parsons et al.*, 2006). We collected ground magnetic data at Anomaly B in order to delineate these features and to compare the resulting map with contoured aeromagnetic data.

Anomaly B is located within the Amargosa Valley, a relatively flat sedimentary basin characterized by alluvial fans, dry washes, sand dunes, and sage brush. The basin is surrounded by mountains that provide sediment to the basin at a rate of about $0.01 - 0.1$ mm per year (*Langenheim et al.*, 1993; *Stamatakos et al.*, 1997; *O'Leary*, 2007). The desert pavement around Anomaly B consists of sand to cobble-sized fragments of weathered tuffs and basalts from nearby Yucca Mountain and Paleozoic-aged meta-sedimentary rocks from hills located East of the Gravity Fault (*Brocher et al.*, 1993) (Figure 1). Parts of the basin are fault-bounded, indicating that this depocenter partially formed by $E - W$ extension across the Bare Mountain Fault, the Gravity Fault (*Ferrill et al.*, 1996; *Thompson*, 2000) and other related structures (*Blakely et al.*, 1999). A large portion of the basin is filled with Miocene ignimbrite deposits generated by massive caldera-forming eruptions of Timber Mountain, located north of Yucca Mountain. A marked shift in the regional style of volcanism is highlighted by the dominance of small-volume, basaltic eruptions during the last 8 Ma.

Magnetic anomalies due to buried sources in the YMR were first identified as early as 1968 (*Bath*, 1968). Following this initial work, in 1978 (*Kane & Bracken*, 1983) and in 1999 (*Blakely et al.*, 2000) aeromagnetic surveys were flown at $120 - 150$ m elevation using line spacings of 400 m. In 2004, a helicopter magnetic survey was flown at an elevation of 30 m by Geophex, Ltd (*Cogbill*, 2004), which overlapped some previously identified magnetic anomalies including the northernmost fraction of Anomaly B. Data from these aeromagnetic surveys suggest that Anomaly B is the largest of five identified magnetic anomalies in the basin, reversely magnetized, with a peak-to-peak amplitude and wavelength of approximately 700 nT and 1 km, respectively. Models using the 1978 survey data and a north-south ground magnetic profile placed the source of Anomaly B at depths less than 250 m and possibly shallower than 150 m (*Langenheim et al.*, 1991, 1993). These models by *Langenheim et al.* (1993) are in good agreement with well log data from two exploration boreholes (Felderhoff Federal drill holes 25-1 and 5-1) near Anomaly B (*Carr et al.*, 1995) that reveal basalt at shallow depths overlying alluvium and tuff. Specifically, well log 25-1 (see Figure 2) shows basalt beginning at approximately 100 m depth beneath an alluvial package. Massive basalt extends to a depth of approximately 150 m, below which the section is once again characterized by alluvium with abundant tuff fragments. Thick layers of tuff, predominantly from the Timber Mountain caldera located 50 km to the north, are intercalated with deposits from other regional volcanoes and extend from approximately 190 m depth to the top of Paleozoic carbonates at a depth of approximately 600 m (Figure 2). This stratigraphic section indicates that the basalt of Anomaly B erupted after the deposition of ignimbrite (tuff) associated with Timber Mountain caldera and other related ignimbrite eruptions beginning 11 Ma (*Carr et al.*, 1995; *O'Leary et al.*, 2002). The Anomaly B basalt erupted onto an alluvial surface, which may have looked similar to today's surface in terms of topography and sedimentation rate. Radiometric age determinations (Ar/Ar) on the basalt from drill hole 25-1 indicate an age of 3.88 ± 0.07 Ma (*Crowe et al.*, 1995), making the reversed magnetization of Anomaly B consistent with the Gilbert reversed chron. This age estimate is also consistent with the estimated age of southeast Crater Flat basalts, cropping out west of Yucca Mountain. Thus, in the area surrounding Anomaly B, well log data suggest an average rate of sediment deposition of approximately 0.04 mm per year, beginning with the eruption of basalt to the present; the source for most of the sediment is Forty Mile Wash, approximately 8 km to the NNW (Figure 1).

Assuming a correlation between Paleozoic-age carbonate rocks in the two boreholes (*Carr et al.*, 1995), offset across the Gravity Fault (Figure 1) appears to be at least 350 m, with little or no offset since the deposition of basalts. Location of the Gravity Fault (Figure 1) is largely inferred from gravity data, which indicate a down-to-the-west displacement in basement. Assuming a normal fault (*Brocher et al.*, 1993; *O'Leary et al.*, 2002), the fault trace lies east of borehole 5-1. Well log 5-1 reports a possible fault zone at 420–440 m depth, within

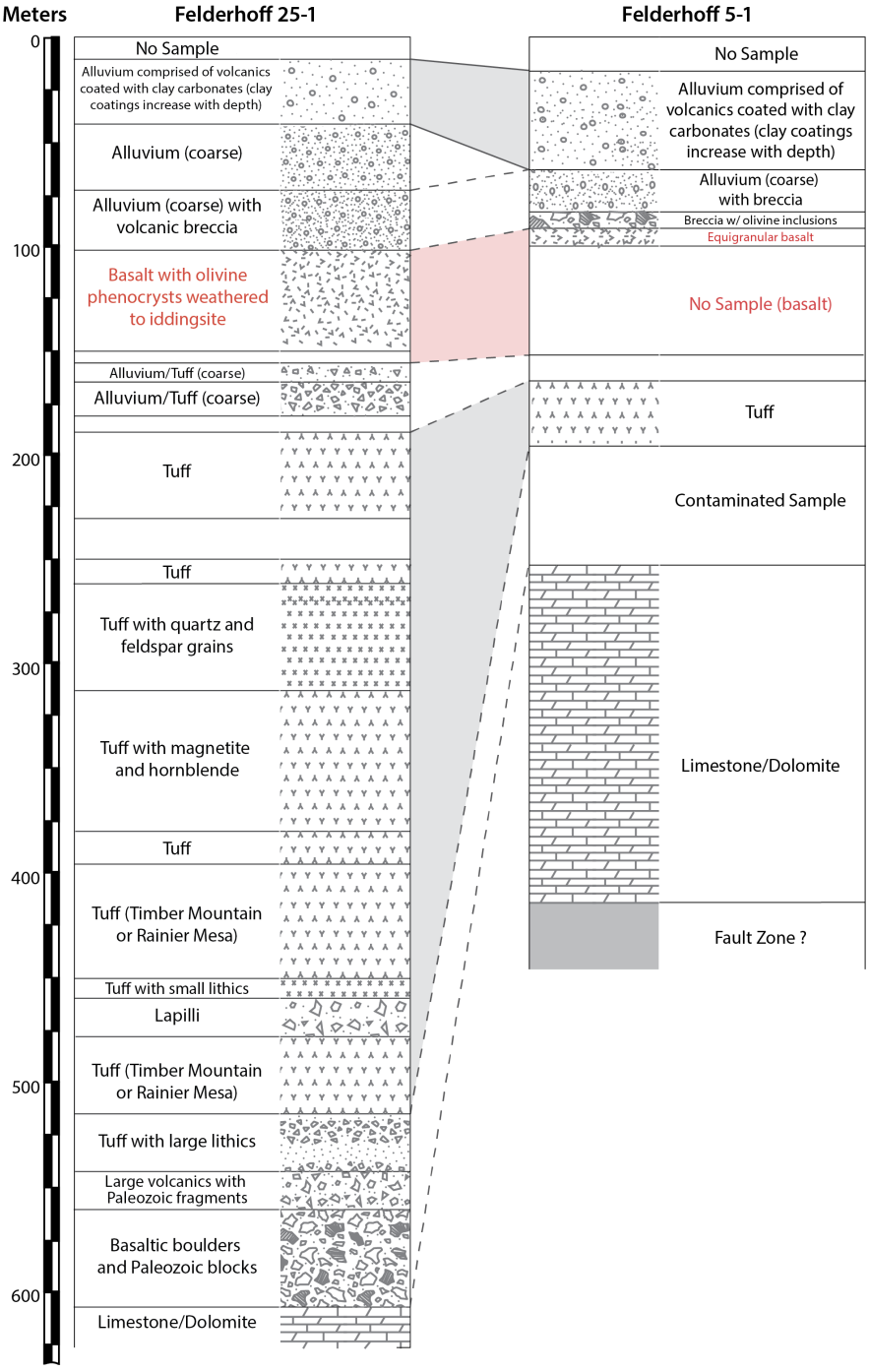

Figure 2: Two stratigraphic columns drawn from well logs described by *Carr et al.* (1995) show the presence of buried volcanic deposits and provide evidence for active faulting between the deposition of Miocene ignimbrites (reported as tuffs in well logs) and Pliocene basalts. In well 25-1, the basalts are first confirmed at a depth of approximately 100 m; in log 5-1 they are first reported at about 90 m depth (both shown in red). Well locations are shown in Figure 1 and have UTM (Zone 11 N WGS84) coordinates: well 5-1: 555278 E 4049833 N and well 25-1: 552806 E 4052592 N.

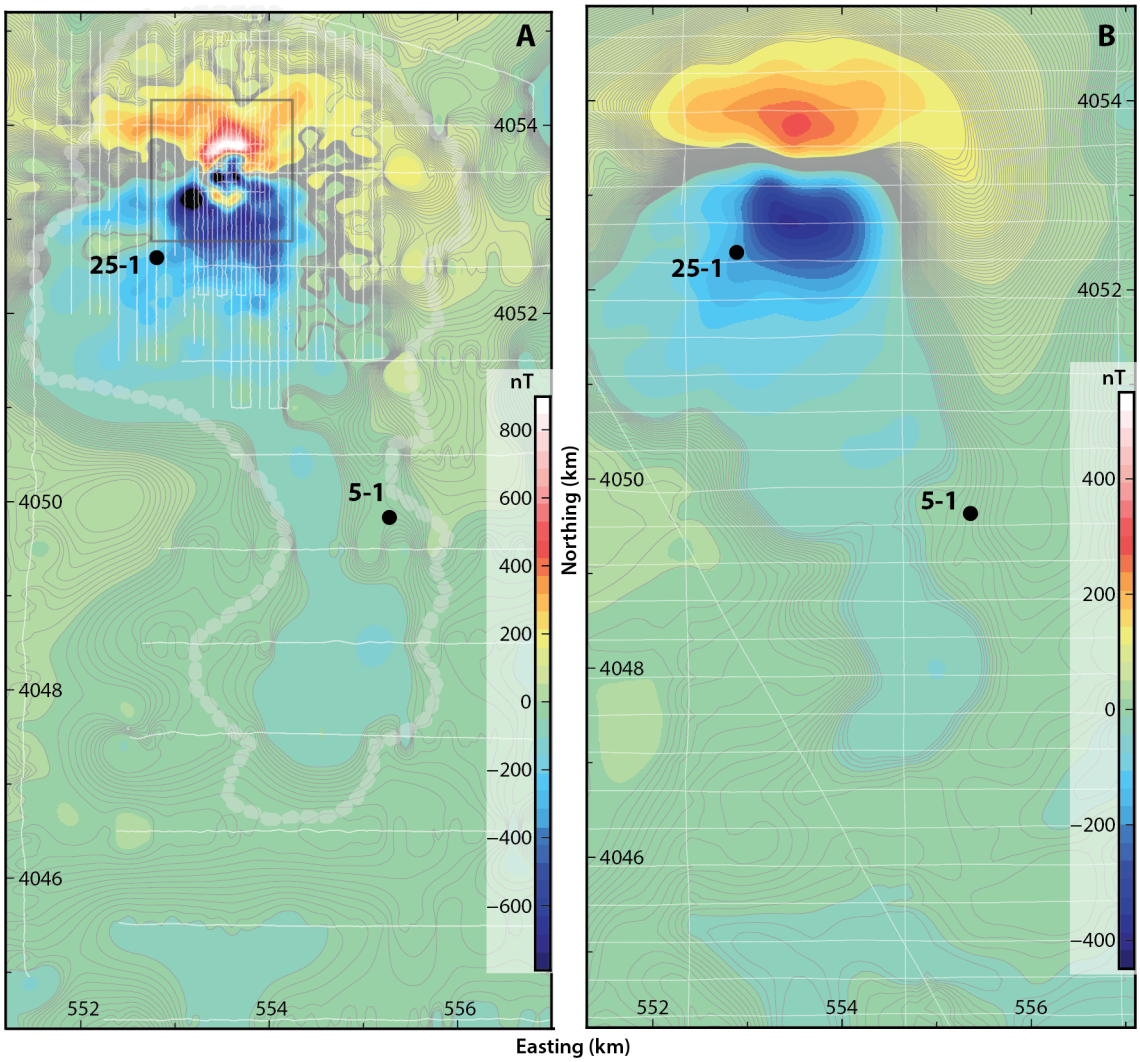

Figure 3: The map pattern of Anomaly B is evident in both the ground magnetic data (A) and aeromagnetic data (B). The ground magnetic survey reveals complexities not expressed in the aeromagnetic survey, especially in the area of the crater rim of the volcano, highlighted by the complex reversely magnetized anomaly centered at 553350 E, 4053350 N. This anomaly is absent in the aeromagnetic data. White lines on each map show the locations of walk lines (map A) and flight lines (map B). Contour intervals for the ground magnetic map (A) and the aeromagnetic map (B) are 4 nT and 2 nT, respectively; contour lines are not shown in the highest amplitude areas. The color scale of both maps is adjusted to facilitate comparison of the mapped anomalies, given that the magnetic signal attenuates with height between the ground surface and the elevation of the aeromagnetic flight lines. Black dots show well locations (see Figures 1 and 2); the gray square outlines the subset of data used for inversion; the thick white dashed line outlines the estimated border of the lava flow.

the limestone. Conspicuously absent from well log 5-1 are the numerous ignimbrite (tuff) layers that form a large part of the sequence seen in well log 25-1 (Figure 2), suggesting that ignimbrites were topographically confined in the basin west of borehole 5-1, or were eroded into the basin before basalt deposition (*Carr et al.*, 1995). The spatial relationship between Anomaly B and the Gravity Fault is potentially important to volcanic hazard assessments; if magma exploited the fault zone during its ascent, then the spatial relationship between Anomaly B and the Gravity Fault could influence the potential location of future volcanism.

Data collection methods

A high-resolution, ground-based, magnetic survey of Anomaly B was conducted during March $25-30$, 2014, between 4051000 m South, 4055000 m North, 551900 m West and 555200 m East (WGS84,UTM zone 11 N). Two teams of 3 persons, each operating a cesium vapor magnetometer (Geometrics G858) concurrently with a GPS data logger/receiver (GlobalSat DG100), ran the survey in parallel, collecting magnetic and GPS data at 1 Hz. One team member navigated with a hand-held GPS, another took notes and periodically checked the equipment, and one carried the instrumentation, a vertically-oriented magnetometer sensor mounted approximately 3 m above the ground on a vertical pole affixed to an aluminum-frame backpack; the data logging GPS was also affixed to this backpack. The vertical orientation of the magnetometer sensor and its 3 m elevation above ground reduced interference from shallow magnetic sources, such as tuff fragments in the alluvium. Data collection, totaling more than 130,000 measurements, occurred along 42 $N-S$ lines spaced 100 m apart along the eastern and western boundaries of the anomaly, and spaced 50 m apart over the central portion of the anomaly; lines ranged in length from $2-4$ km (Figure 3). Seven $E-W$ lines, each 0.7 km in length, crossed the central portion of the anomaly.

Additionally, in 2011, using the same instrumentation, approximately 40,000 measurements were made along 10 $E-W$ lines spaced approximately 1 km apart and along one $N-S$ line. The 2011 data helped to constrain the southern extent of the anomaly, and facilitated comparison with the aeromagnetic data (Figure 3); the aeromagnetic data are available from *USGS* (2001).

Data processing

Magnetic data were downloaded using the Magmap2000 software by Geometrics, Inc., and software by GlobalSat was used to download the GPS data. Preliminary analyses were conducted on-site to assess data quality and to actively plan the survey. The work flow used to generate the final data product is illustrated in Figure 4 and proceeds as follows. The time of collection for both magnetic and GPS measurements is converted to a decimal time format. Raw magnetic observations are corrected for data drift. Magnetic and GPS observations are georeferenced using time-stamp matching, resulting in an x, y location for each magnetic reading. Latitude, longitude coordinates are converted to UTM coordinates. The collated data are processed using an algorithm for despiking and by subtraction of an average International Geomagnetic References Field (IGRF) value from the observations. The computer codes (written in PERL) to implement this work flow are provided as text files in the supplementary material, including metadata for the survey and all pre-processed and post-processed survey data.

To resolve variations in the measured magnetic field unrelated to the signal of interest, a drift correction was applied using values of Earth's magnetic field recorded at the Boulder Magnetic Observatory in Colorado (≈ 1050 km distant). These quality controlled magnetic field readings are continuously recorded at one minute intervals and referenced to Greenwich Mean Time (GMT). Due to the insignificant variations in the drift on a minute-to-minute basis during the data collection period, it was unnecessary to interpolate the drift corrections at one second intervals prior to applying them to the 1 Hz survey data. Although the Fresno

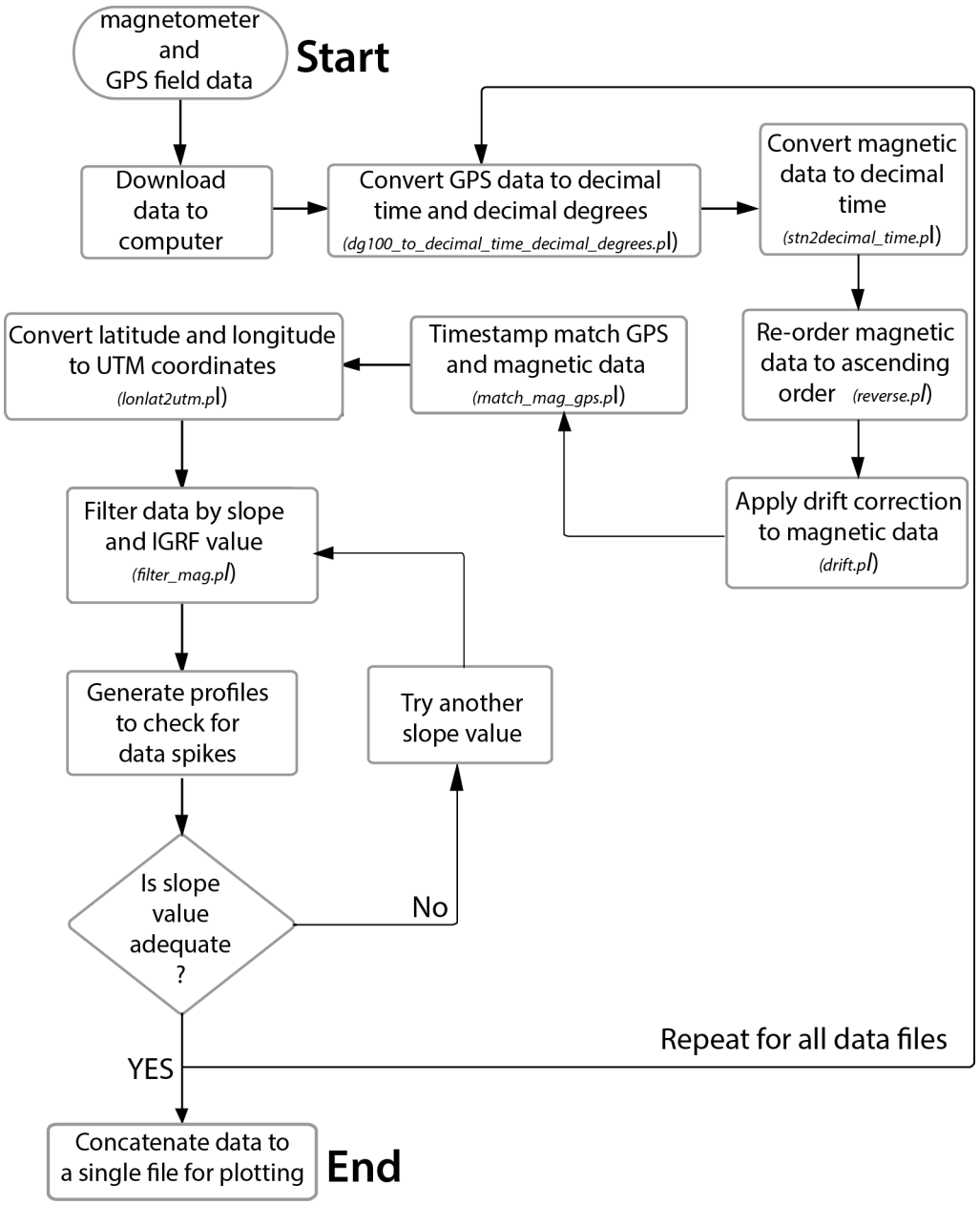

Figure 4: The magnetic and GPS survey data are processed following the START to END procedure outlined in this flow chart. The steps between converting the GPS data format and filtering the data by slope are accomplished by executing the PERL scripts (*.pl) named in the flow chart.

Magnetic Observatory (California) is closer to the survey area (≈ 302 km distant), the Boulder station readings were chosen for drift correction because magnetic readings each minute were available during the entire field survey, whereas the Fresno Observatory showed data gaps during the survey period. A comparison of magnetic readings during identical times from both observatories showed similar values (± 5 nT) during the intervals of data collection.

Drift-corrected magnetic data were obtained by differencing the observatory background reading and the magnetic observation at time t, the time nearest to collection of individual survey readings:

$$M_{drift} = M_{avg} - M_t \tag{1}$$

where M_{drift} is the drift correction (nT), M_{avg} is the average magnetic reading at the observatory, and M_t is the magnetic reading at the observatory at time t. The drift-corrected magnetic reading is obtained by:

$$M_{drift-corrected} = M_{observed,t} + M_{drift} \tag{2}$$

where $M_{drift-corrected}$ is the drift-corrected survey reading (nT) and $M_{observed,t}$ is the observed survey reading at time t. Overall, the survey period was magnetically quiet, with a maximum daily drift of approximately 40 nT.

Magnetic measurements were located by time-stamp matching the decimal time output of the GPS with that of the magnetometer; only those data points that time matched to within one second were retained after this processing step. Original GPS locations were collected in degrees and decimal minutes and converted to UTM coordinates using the *proj*.4 cartographic projections library originally developed by *Evenden* (1995) at the U.S. Geological Survey (*PROJ.4 Development Team*, 2014) and the *gdal* open source geospatial data abstraction library (*GDAL Development Team*, 2014).

Accurate interpretation and modeling of magnetic anomalies can be hindered by sensor dropouts and spikes in the data associated with anomalous sensor behavior (such as inappropriate sensor orientation or jarring of the sensor during data collection) or anthropogenic magnetic noise sources. Although infrequent during this survey, steps were taken to ensure that dropouts and spikes were minimized in the final data product. Subjective analysis of various filtered and unfiltered profiles within the survey area showed that limiting the slope between neighboring observation points to $< 75\,\mathrm{nT\,m^{-1}}$ did an excellent job of removing most data spikes (compare Figures 5A and B). Data points that created profile slopes $\geq 75\,\mathrm{nT\,m^{-1}}$ were deleted from the data set.

Prior to concatenating all files into the final product, the anomalous field was calculated by subtracting the average IGRF value during the survey periods (49083.5 nT and 49351.4 nT for the 2014 and 2011 surveys, respectively) from each data point. Magnetic measurements from the 2011 survey were also processed to correct for data spikes, dropouts (values equal to zero) and the IGRF value; no drift correction was applied.

Daily processing was automated through use of a master script, which takes as input the UTM zone of the survey, the slope used in the filter, and the IGRF value. The individual scripts necessary for carrying out each step (see Figure 4) were accessed through this master script. The final data file contains the UTM location (Easting, Northing) and processed magnetic value for each measurement. The processed magnetic values range from approximately -1000−1000 nT, resulting in a 2000 nT variation about the IGRF value. Survey error was assessed by comparing magnetic readings obtained at line-crossings (Figure 3A). Survey error is defined as the standard deviation of the differences in processed magnetic values measured at locations < 5 m apart and separated in time by more than 30 minutes. The mean variation observed was 0.8 nT with a standard deviation of 44 nT (Figure 6); this variation is due to a high magnetic gradient within the survey area and the occurrence of magnetized tuff and basalt fragments in the shallow sub-surface.

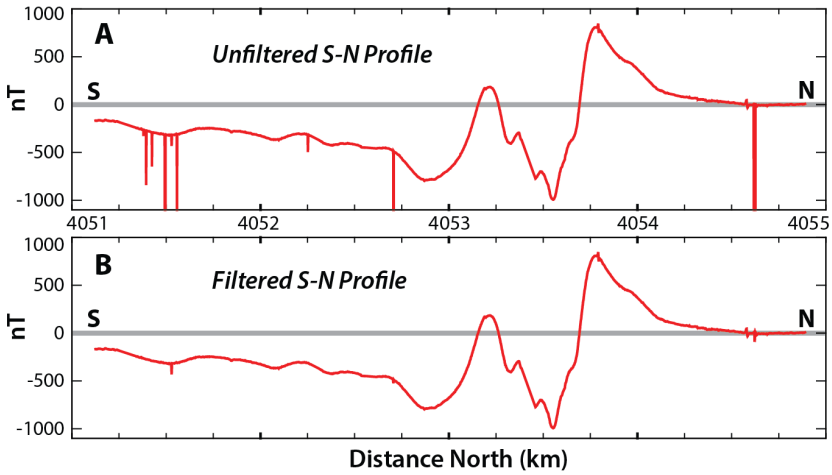

Figure 5: A south-to-north profile of ground magnetic data collected through the center of Anomaly B (553600 E ±5m) shows the IGRF value subtracted from each reading and a drift correction applied. Unfiltered data have several large amplitude spikes (A), which are removed or strongly attenuated by filtering (B). The auto-correction used a < 75 nT/m slope filtering algorithm between neighboring data points to remove data spikes and dropouts; see file *filter_mag.pl*.

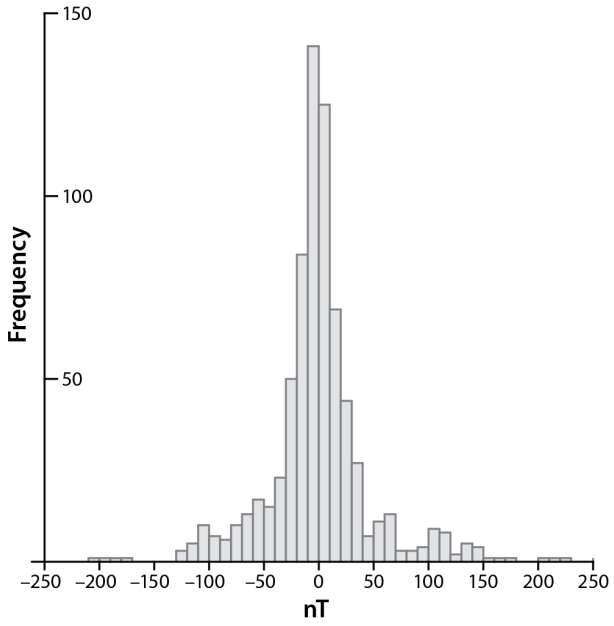

Figure 6: Differences in processed magnetic values for the 2014 survey, measured at locations < 5 m apart and separated in time by more than 30 minutes, are binned and plotted. The mean difference among these magnetic readings is 0.8 nT with a standard deviation of 44 nT. This survey error of 44 nT is due to the high magnetic gradient within the survey area, especially near the interpreted crater rim area, and the occurrence of magnetized tuff and basalt fragments in the alluvium of the shallow sub-surface.

Survey results

Interest in the Yucca Mountain Region as a potential nuclear waste repository site led to extensive surveys of the area using various geological and geophysical methods. Discovered during previous aeromagnetic surveys, Anomaly B was further investigated via helicopter aeromagnetic, ground magnetic profiles, gravity, and well explorations (*Langenheim et al.*, 1991, 1993; *Carr et al.*, 1995; *Grauch et al.*, 1997; *Blakely et al.*, 1999, 2000; *USGS*, 2001; *O'Leary et al.*, 2002; *Perry et al.*, 2005). These earlier studies highlighted the broad-scale features of Anomaly B and hinted at finer scale intricacies, which are revealed in greater detail using the ground magnetic data from this study. Anomaly B is centered at 553350 E, 4053350 N (UTM zone 11 N) and covers a map distance of approximately 4.5 km in the $E-W$ direction and 8.5 km in the $N-S$ direction. The bulk of this anomalous signal is dominated by a negative anomaly which extends from the center of the anomaly to about 7 km south. The peak amplitude based on the ground magnetic survey is located within the crescent-shaped region near the center and is approximately −1000 nT (Figure 3A). The strongest positive signals associated with Anomaly B are confined to a smaller region (approximately 1 km^2) to the north of the negative signal. The positive portion of Anomaly B is roughly semicircular with small lobes protruding from the northwestern and northeastern sides while a large lobe drapes down the eastern side from 4054000 N to about 4052000 N. Peak amplitude of the positive signal is about +900 nT.

The dipolar nature of the mapped magnetic anomaly, resulting in an overall positive anomaly to the north and overall negative anomaly to the south, is consistent with an isolated buried magnetic source of uniform magnetization. Its amplitude and wavelength, together with the occurrence of basaltic rocks in the two well logs, lead us to agree with previous investigators and interpret the anomaly as caused by a buried volcanic vent. The irregular edges of the anomaly, defined by high magnetic gradients, and lobate structure associated with both the negative and positive signals are interpreted to reflect the maximum extent of the lava flow field erupted from a central volcanic vent. Thus, the lava flow field is interpreted to have a minimum diameter ≈ 4.5 km and a maximum flow length of approximately 7 km extending south from the vent. This lava flow field likely consists of numerous cooling units, but any change in chemistry between cooling units does not appear to substantially affect the remanent magnetization to the point where changes are observed across the magnetic map. Rather, the entire flow field can be considered to be uniformly magnetized.

The total volume of basalt associated with Anomaly B is estimated from the lateral extent of the anomalous signal (Figure 3A) and from an estimation of lava flow thickness based on the thickness of basaltic rocks (50 m) in the Felderhoff Federal drill holes (Figure 2). The lateral extent of the lava flow field was determined visually based on inflection points in magnetic profiles along $E-W$ survey lines across the anomaly. The volume estimate includes the vent area and its associated lavas (24 km^2, Figure 3A) and is found to be approximately 1.2 km^3.

Details in the subsurface are evident on the ground magnetic map where data collection occurred at 50 m spacing over the central portion of Anomaly B; circular features, interpreted to be the location of the vent complex, are revealed (Figure 3A). The rim-to-rim crater diameter, indicated by the oscillation of the positive and negative signals at the center of Anomaly B, is about 700 m. Within this area, the two strong negative (approximately -1000 nT each) signals may be caused by the presence of additional vents. An interesting exercise is to compare the general map view of Anomaly B with the map patterns of volcanoes that are exposed at the surface in the region. Thirsty Mesa is a 4.63 ± 0.02 Ma (*Fleck et al.*, 1996) shield volcano located approximately 50 km north of Anomaly B. Thirsty Mesa has a lava flow field approximately 7 km in diameter and 60 m thick. Several vents comprise the eruptive center with an overall rim-to-rim diameter of approximately 770 m. The magnetic anomalies associated with lava flows that comprise the slopes of Thirsty Mesa create a mottled pattern in map view (*Grauch et al.*, 1997) quite similar to the wavelengths of complex magnetic anomalies in the vent area of Anomaly B (Figure 3A). This comparison suggests that Anomaly B is a shield volcano complex, with multiple vents and a compound lava flow field that extends away from the vent complex in all directions, but

extends furthest to the south. In contrast, the younger scoria cones in the area are of significantly smaller volume and have correspondingly smaller vent and cone diameters. For example, Lathrop Wells volcano has a crater radius of approximately 140 m, cone width of 610 m, and maximum lava flow length of 2 km, typical for scoria cones in the region. Further north, NE and SW Little Cones, approximately 1 Ma old volcanic centers, have basal diameters of 230 m and 350 m, respectively. As was the case with Anomaly B and Thirsty Mesa, these centers show numerous short-wavelength magnetic signals superimposed on the broader anomalous signal. In the case of SW Little Cone, *Stamatakos et al.* (1997) show that the short-wavelength anomalies are associated with buried lava flows in the vicinity of the breached flank of the cone. Table 1 compares the dimensions of Anomaly B with mapped volcanoes in the Yucca Mountain Region (*Valentine & Perry*, 2006).

Table 1: Summary table of cone, crater and lava flow dimensions associated with some of the lava flows of the Yucca Mountain Region. Thirsty Mesa and Anomaly B are interpreted to be shield volcanoes, and so cone width is not indicated.

Volcano	**Cone Width** (m)	**Crater Width** (m)	**Lava Flow Length** (km)	**Volume** (km^3)
Lathrop Wells	610	140	2	0.1
Red Cone	540	110	1.7	0.04
Black Cone	700	130	2.1	0.05
Little Black Peak	400	110	1.5	0.02
Hidden Cone	700	150	1.6	0.03
Thirsty Mesa	-	770	7.1	2.6
Anomaly B	-	700	7	1.0

The ground magnetic map places the anomaly and interpreted crater area in the hanging-wall of the Gravity Fault (Figure 1). Although the exact location of the trace of the Gravity Fault at the surface is uncertain, it appears that the the crater area is approximately 3 km west of the fault trace. This suggests that magma may have followed the fault zone during ascent through the brittle crust, and broken out of the fault zone into the hanging-wall at shallow depth.

Inversion

Non-linear inversion was performed using a subset of the ground magnetic data enclosing a region centered on the crater rim (outlined as a gray box in Figure 3A) using the downhill simplex method (*Nelder & Mead*, 1965); the algorithm minimizes a function of N model parameters needed to generate a geologically reliable model. For this inversion, it is assumed that the buried volcano can be represented by $100\,m^2$ vertically-sided prisms. Consequently, the map area (Figure 7A) is subdivided into a total of 256 prisms. The inversion procedure allows prism heights (depth to top) to vary, however, all prisms are required to have a uniform base that assumes a flat desert pavement upon which the lavas were originally erupted. This depth to base of the prisms is adjusted during inversion. Finally all of the prisms are assumed to have the same vector of remanent magnetization, defined by inclination, declination and intensity of magnetization. Thus, the model may vary a total of 260 parameters. For this inversion the magnetic susceptibility is assumed to be zero, as the intensity of remanent magnetization is many times the susceptibility, with measured Königsberger ratios for some YMR basalts of $10 - 70$ (*Stamatakos et al.*, 2007).

Briefly, this inversion method calculates a forward solution for 261 $(N + 1)$ randomly-generated parameter sets using the analytical solution for the magnetic field produced by a buried prism derived by *Rao & Babu* (1991). Model values, initially chosen randomly from specified parameter ranges, are used to calculate the magnetic anomaly. Calculated magnetic values and observed magnetic data for each of these forward solu-

tions are compared using the a root mean squared error (RMSE) goodness-of-fit test. The parameters are then systematically adjusted (within specified ranges) until the RMSE varies < 0.005 nT between subsequent iterations. Typically, tens of thousands of iterations are performed to identify this minimum. Local minima are identified by altering the ranges for input parameters based on the output of previous models and by comparing a normalized RMSE. Models of potential field data are susceptible to issues of equivalency. In this case, magnetic variation in the anomaly map of the crater area (Figure 7A), might be explained by a relatively deep, large-volume structure of lower intensity of magnetization (Figure 7B), or by a shallow, relatively small-volume structure of high intensity of magnetization (Figure 7C). We explore these possibilities using two different sets of input parameter ranges. In the first model, we specify a range for the intensity of magnetization of $1-6$ Amp m^{-1}, corresponding to a range of magnetic intensities measured for several basalt units in the region, including those associated with Anomaly A (*Stamatakos et al.*, 2007, Figure 1). The input range for depth to base of the prisms varies between $100-199$ m and depth to top of the prisms is allowed to vary between $20-199$ m, with the requirement that depth to prism top not exceed depth to prism base. The best-fit solution for this model (Figure 7B) yields an intensity of magnetization of approximately 6 Amp m^{-1}, with depth to prism base at 197 m below ground surface. This inversion model suggests that depth to top of the crater rim is as shallow as 33 m; the inclination and declination of remanent magnetization are estimated to be -57° and 185°, respectively (Figure 7B).

An alternative inversion model was constructed specifying a higher range for the intensity of magnetization, $10-17$ Amp m^{-1}, and a shallower range for prism depth. This intensity of remanent magnetization corresponds to the range of measured values in some outcropping YMR basalts, including basalts of SE Crater Flat and the Little Cones (*Champion*, 1991; *Stamatakos et al.*, 1997; *La Femina et al.*, 2002). Specifically, depth to prism base is allowed to vary $60-150$ m, while depth to prism top varies $10-150$ m, again with the requirement that depth-to-top not exceed depth-to-base. For this range of input parameters, the inversion model estimates the prism base to be 147 m; the tallest prism on the crater rim reaches a depth of 70 m; the inclination and declination of remanent magnetization is estimated to be -47° and 180°, respectively; the intensity of remanent magnetization is about 16 Amp m^{-1} (Figure 7C). In this model, the depth estimates are in excellent agreement with reports of depth to the base of the basalt (150 m) in the two well logs (Figure 2).

These two inversions represent a possible range of acceptable models based on identical magnetic data. The RMSE for these models is essentially identical (82.4 and 91.2 nT, respectively). Both models have residuals that are generally random, but with slightly higher amplitudes associated with very short-wavelength anomalies in the crater rim area (difference maps, Figures 7B and C). Similarly, *(i)* all inversion models require a shallow depth to the crater rim (< 100 m), *(ii)* all inversion models yield a crater diameter of approximately 700 m (Figures 8A and B), *(iii)* most models indicate that the shallowest part of the structure, interpreted to be the highest parts of the buried crater rim, are on the west and north sides, and *(iv)* most models suggest that the crater may have two vents, located $E-W$ from one another and separated by a narrow septum.

Models of lower remanent magnetization require a larger lava volume and greater depth to base. We favor the model with the higher remanent magnetization of 16 Amp m^{-1} (Figures 8B) because this model agrees with the depth to base of the basalt layer identified in the two well logs. This model allows for rapid fluctuation in depth-to-top of the prisms on the lava flow field (Figures 8A and B), which we interpret to result from equivalence of the magnetic signal produced by different prism geometries. That is, the magnetic signal produced by a tall prism adjacent to a short one can yield a similar calculated anomaly compared to the calculated anomaly resulting from two adjacent medium-sized prisms. In this model, it was necessary to utilize relatively small-area prisms (100 m^2) to capture the complexity of the magnetic anomaly in the inferred crater area. However, small-area prisms produced rapid fluctuations in the thickness of the lava flow field, which may not reflect the flow's true geometry. The model with higher remanent magnetization (Figures 8B) is used to estimate lava flow thickness away from the vent area to be 42 ± 15 m. This yields a total volume of the Anomaly B crater area and lava flows of 1.0 ± 0.4 km^3.

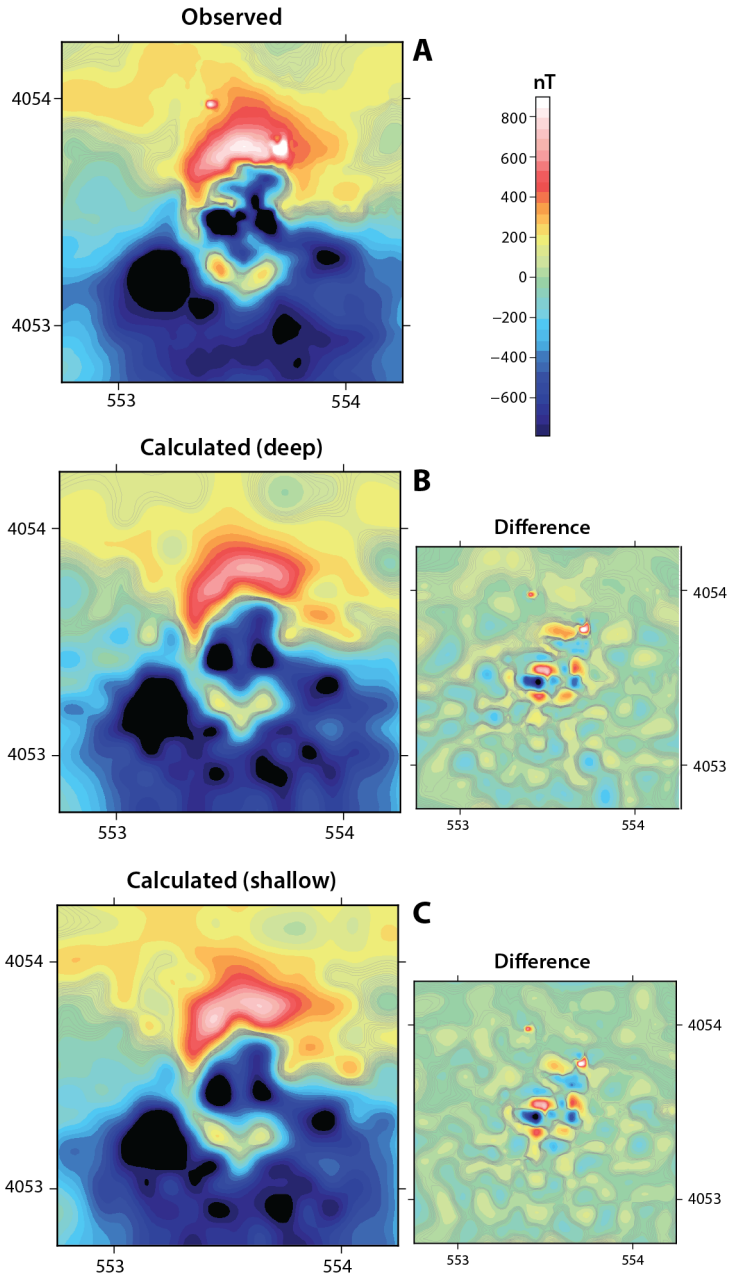

Figure 7: Magnetic inversion results. (A) Map of observed magnetic data; these data are modeled by inversion of a model in which prisms are $100\,\mathrm{m}^2$ in planimetric area, of uniform depth to the base and uniform magnetization, and of varying heights. (B) Best-fit calculated anomaly specifying a relatively low remanent magnetization ($6\,\mathrm{Amp\,m}^{-1}$) and difference with observed magnetic values. (C) Best-fit calculated anomaly specifying a relatively high remanent magnetization ($16\,\mathrm{Amp\,m}^{-1}$) and difference with observed magnetic values. See model geometries in Figures 8a and b.

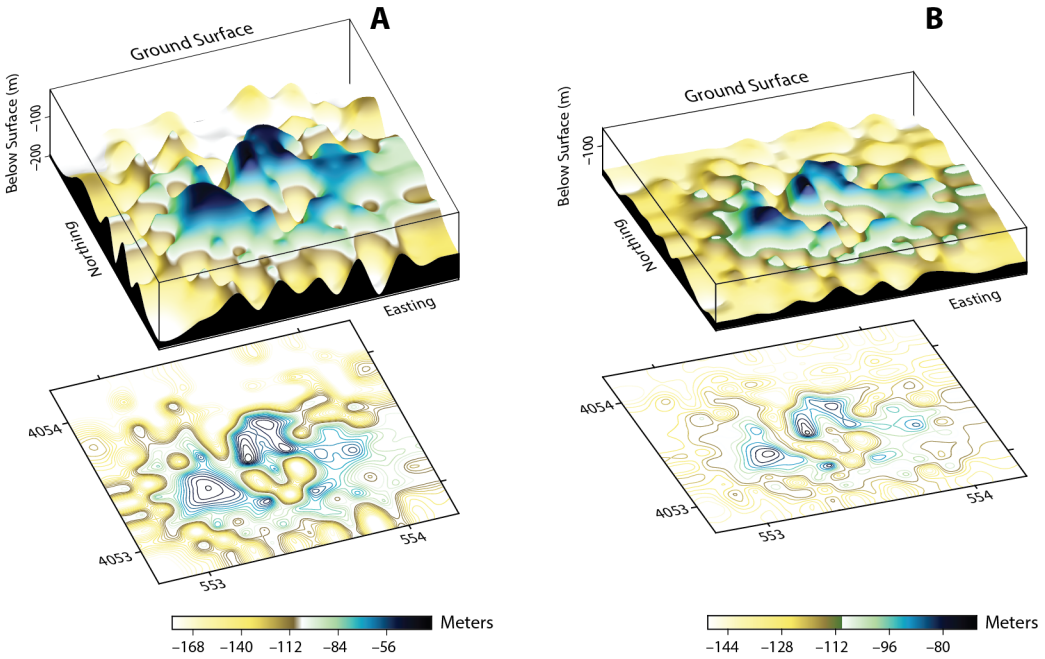

Figure 8: Oblique perspective view of two possible 3D models for the buried structure that produces Anomaly B. Model **A** places the base of the uniformly magnetized volcano on a flat surface at a depth of 197 m and the crater rim at a minimum depth of approximately 33 m beneath the ground surface, assuming a remanent magnetization of 6 Amp m^{-1}. Model **B** has a shallower depth to base (147 m) assuming a higher remanent magnetization (16 Amp m^{-1}). In both models, rapid changes in lava thickness away from crater area may reflect model uncertainty or actual changes in lava thickness. For model **B**, lava thickness is estimated to be 42 ± 15 m.

Conclusions

In areas with high sedimentation rates such as the Amargosa Valley, volcanic features may be buried in geologically short time frames. This fact has strong implications for volcanic hazard assessments, particularly in regions with low rates of volcanism, because the addition or removal of a single event may cause significant variation in estimates of future eruption probabilities. Potential-field data gathered during magnetic and gravity surveys offer a method for identifying buried structures. Such is the case for Anomaly B, which has been surveyed using ground-based and aeromagnetic techniques. High-resolution, ground-based magnetic surveying of Anomaly B has allowed us to estimate depth of burial (147 m), and hence sedimentation rate (0.04 mm yr^{-1}), and eruption volume ($1.0 \pm 0.4\,km^3$), which is greater than the volume estimated by *Langenheim et al.* (1993) using aeromagnetic data ($0.1-0.4\,km^3$).

These estimates and analyses, useful for understanding the time-volume relationships in this basalt volcanic field, require the collection of relatively high-resolution data, as illustrated here using the comparison of aeromagnetic and ground magnetic maps. Our workflow, including specific PERL scripts created for individual processing steps, may facilitate such analyses in other volcanic fields.

Acknowledgments

The authors thank Mark Bebbington for editorial supervision of this manuscript and two anonymous reviewers for their valuable comments. Catie Cater, Jay Ayer, and Brian Ferwerda participated in collection of the 2011 data set. We thank Estella Atekawa and the geophysics group at Oklahoma State University for lending us their cesium-vapor magnetometer. These data were collected

as part of a graduate geophysics course at the University of South Florida. Generic Mapping Tools was used to create some figures in the paper (*Wessel & Smith*, 1998).

References

Bath, G. D. (1968) Aeromagnetic anomalies related to remanent magnetism in volcanic rock, Nevada Test Site. *Geological Society of America Memoirs*, **110**:135–146. 2, 3, 4

Bebbington, M. S. (2013*a*) Assessing spatio-temporal eruption forecasts in a monogenetic volcanic field. *Journal of Volcanology and Geothermal Research*, **252**:14–28. 2

Bebbington, M. S. (2013*b*) Models for temporal volcanism. *Statistics in Volcanology*, **1**:1–24. URL scholarcommons.usf.edu/siv/vol1/iss1/1. 2

Bebbington, M. S. & Cronin, S. J. (2011) Spatio-temporal hazard estimation in the Auckland Volcanic Field, New Zealand, with a new event-order model. *Bulletin of Volcanology*, **73**(1):55–72. 2

Becerril, L., Cappello, A., Galindo, I., Neri, M. & Negro, C. Del (2013) Spatial probability distribution of future volcanic eruptions at El Hierro Island (Canary Islands, Spain). *Journal of Volcanology and Geothermal Research*, **257**:21–30. 2

Blakely, R. J., Jachens, R. C., Calzia, J. P. & Langenheim, V. E. (1999) Cenozoic basins of the Death Valley extended terrane reflected in regional-scale gravity anomalies. *In* L.A. Wright & B.W. Troxel (eds.) *Cenozoic Basins of the Death Valley Region*, Special volume 333, 1–16. Geological Society of America, Boulder, Co. 4, 11

Blakely, R. J., Langenheim, V. E., Ponce, D. A. & Dixon, G. L. (2000) Aeromagnetic survey of the Amargosa Desert, Nevada and California: A tool for understanding near-surface geology and hydrology. Open-File Report 00–188, United States Geological Survey. 2, 3, 4, 11

Brocher, T. M., Carr, M. D., Fox, K. F. & Hart, P. E. (1993) Seismic reflection profiling across Tertiary extensional structures in the eastern Amargosa Desert, southern Nevada, Basin and Range province. *Geological Society of America, Bulletin*, **105**(1):30–46. 4

Cappello, A., Neri, M., Acocella, V., Gallo, G., Vicari, A. & Negro, C. Del (2012) Spatial vent opening probability map of Etna volcano (Sicily, Italy). *Bulletin of Volcanology*, **74**(9):2083–2094. 2

Carr, W. J., Grow, J. A. & Keller, S. M. (1995) Lithologic and geophysical logs of drill holes Felderhoff Federal 5-1 and 25-1, Amargosa Desert, Nye County, Nevada. Technical report, USDOE Nevada Operations Office, Las Vegas, NV. 3, 4, 5, 7, 11

Champion, D. E. (1991) Volcanic episodes near Yucca Mountain as determined by paleomagnetic studies at Lathrop Wells, Crater Flat, and Sleeping Butte, Nevada. *In High Level Radioactive Waste Management: Proceedings of the second annual international conference*, volume 1, 61–67. American Nuclear Society, Las Vegas, Nv. 13

Cogbill, A. (2004) Helicopter aeromagnetic survey Yucca Mountain, Nevada. *In Probabilisitic Volcanic Hazard Analysis Update, Yucca Mountain Project: Workshop*, volume 1, J. 4

Connor, C. B. & Connor, L. J. (2009) Estimating spatial density with kernel methods. *In* C.B. Connor, N.A. Chapman & L.J. Connor (eds.) *Volcanic and Tectonic Hazard Assessment for Nuclear Facilities*, 346–368. Cambridge University Press, Cambridge, UK. 2

Connor, C. B. & Hill, B. E. (1995) Three nonhomogeneous Poisson models for the probability of basaltic volcanism: application to the Yucca Mountain region, Nevada. *Journal of Geophysical Research: Solid Earth (1978–2012)*, **100**(B6):10107–10125. 2

Connor, C. B., Lane-Magsino, S., Stamatakos, J. A., Martin, R. H., Femina, P. C. La, Hill, B. E. & Lieber, S. (1997) Magnetic surveys help reassess volcanic hazards at Yucca Mountain, Nevada. *Eos, Transactions of the American Geophysical Union*, **78**(7):73–78. 2

Connor, C. B., Stamatakos, J. A., Ferrill, D. A., Hill, B. E., Ofoegbu, G. I., Conway, F. M., Sagar, B. & Trapp, J. (2000) Geologic factors controlling patterns of small-volume basaltic volcanism: Application to a volcanic hazards assessment at Yucca Mountain, Nevada. *Journal of Geophysical Research: Solid Earth (1978–2012)*, **105**(B1):417–432. 2

Connor, L. J., Connor, C. B., Meliksetian, K. & Savov, I. (2012) Probabilistic approach to modeling lava flow inundation: a lava flow hazard assessment for a nuclear facility in Armenia. *Journal of Applied Volcanology*, **1**(1):1–19. 2

Crowe, B., Perry, F., Murrell, M., Poths, J., Valentine, G. A., Wells, S., Bowker, L., Finnegan, K., Geissman, J. & McFadden, L. (1995) Status of volcanism studies for the Yucca Mountain site characterization project. Technical report, Los Alamos National Lab., NM (United States). 2, 4

El Difrawy, M. A., Runge, M. G., Moufti, M. R., Cronin, S. J. & Bebbington, M. (2013) A first hazard analysis of the Quaternary Harrat Al-Madinah volcanic field, Saudi Arabia. *Journal of Volcanology and Geothermal Research*, **267**:39–46. 2

Evenden, G. I. (1995) *Cartographic Projection Procedures for the UNIX Environment: A User's Manual*. 9

Ferrill, D. A., Stamatakos, J. A., Jones, S. M., Rahe, B., McKague, H. L., Martin, R. H. & Morris, A. P. (1996) Quaternary slip history of the Bare Mountain Fault (Nevada) from the morphology and distribution of alluvial fan deposits. *Geology*, **24**:559–562. 4

Fleck, R. J., Turrin, B. D., Sawyer, D. A., Warren, R. G., .Champion, D. E, Hudson, M. R. & Minor, S .A. (1996) Age and character of basaltic rocks of the Yucca Mountain region, southern Nevada. *Journal of Geophysical Research: Solid Earth (1978–2012)*, **101**(B4):8205–8227. 11

GDAL Development Team (2014) *GDAL - Geospatial Data Abstraction Library, Version 1.11.1*. Open Source Geospatial Foundation. URL http://www.gdal.org. 9

Grauch, V. J. S., Sawyer, D. A., Fridrich, C. J. & Hudson, M. R. (1997) Geophysical intepretations west of and within the northwestern part of the Nevada Test Site. Open-File Report 97–476, United States Geological Survey. 2, 11

Hill, B. E., Aspinall, W. P., Connor, C. B., Godoy, A. R., Komorowski, J.-C. & Nakada, S. (2009) Recommendations for assessing volcanic hazards at site of nuclear installations. *In* C.B. Connor, N.A. Chapman & L.J. Connor (eds.) *Volcanic and Tectonic Hazard Assessment for Nuclear Facilities*, 566–592. Cambridge University Press, Cambridge, UK. 2

Hill, B. E., Femina, P. C. La, Stamatakos, J. A. & Connor, C. B. (2002) Preliminary evaluation of the effects of buried volcanoes on estimates of volcano probability for the proposed repository site at Yucca Mountain, Nevada. *In American Geophysical Union Fall Meeting Abstracts*, volume 1, 1225. 2

Ho, C.-H. & Smith, E. I. (1998) A spatial-temporal/3–d model for volcanic hazard assessment: application to the Yucca Mountain region, Nevada. *Mathematical Geology*, **30**(5):497–510. 2

Kane, M. F. & Bracken, R. E. (1983) Aeromagnetic map of Yucca Mountain and surrounding regions, southwest Nevada. Open-File Report 83–616, United States Geological Survey. Scale 1:48,000. 2, 3, 4

La Femina, P. C., Connor, C. B., Stamatakos, J. A. & Farrell, D. A. (2002) Imaging an active normal fault in alluvium by high-resolution magnetic and electromagnetic surveys. *Environmental and Engineering Geoscience*, **8**(3):193–207. 13

Langenheim, V. E., Carle, S. F., Ponce, D. A. & Phillips, J. D. (1991) Revision of an aeromagnetic survey of the Lathrop Wells area, Nevada. Open-File Report 91–46, United States Geological Survey. 2, 3, 4, 11

Langenheim, V. E., Kirchoff-Stein, K. S. & Oliver, H. W. (1993) Geophysical investigations of buried volcanic centers near Yucca Mountain, southwest Nevada. *In High Level Radioactive Waste Management 1993*, 1840–1846. American Society of Civil Engineers. 2, 3, 4, 11, 15

Nelder, J. A. & Mead, R. (1965) A simplex method for function minimization. *The Computer Journal*, **7**(4):308–313. 12

O'Leary, D. W. (2007) Tectonic models for Yucca Mountain, Nevada. *Memoirs of the Geological Society of America*, **199**:105–153. 4

O'Leary, D. W., Mankinen, E. A., Blakely, R. J., Langenheim, V. E. & Ponce, D. A. (2002) Aeromagnetic expression of buried basaltic volcanoes near Yucca Mountain, Nevada. Open-File Report 02–020, United States Geological Survey. 2, 3, 4, 11

Parsons, T., Thompson, G. A. & Cogbill, A. H. (2006) Earthquake and volcano clustering via stress transfer at Yucca Mountain, Nevada. *Geology*, **34**(9):785–788. 4

Perry, F. V., Cogbill, A., Kelley, R., Youngs, R. & Cline, M. (2005) Updating an expert elicitation in the light of new data: Ten years of probabilistic volcanic hazard analysis for the proposed high-level radioactive waste repository at Yucca Mountain, Nevada. *In AGU Fall Meeting Abstracts*, volume 1, 08. 11

PROJ.4 Development Team (2014) Proj.4: Cartographic projections library, version 4.4.6. URL http://trac.osgeo.org/proj/. 9, 22

Rao, D. B. & Babu, N. R. (1991) A rapid method for three-dimensional modeling of magnetic anomalies. *Geophysics*, **56**(11):1729–1737. 12

Rechard, R. P., Wilson, M. L. & Sevougian, S. D. (2014) Progression of performance assessment modeling for the Yucca Mountain disposal system for spent nuclear fuel and high-level radioactive waste. *Reliability Engineering & System Safety*, **122**:96–123. 2

Smith, E. I & Keenan, D. L. (2005) Yucca Mountain could face greater volcanic threat. *Eos, Transactions of the American Geophysical Union*, **86**(35):317–321. 2

Stamatakos, J. A., Biwas, S. & Silver, M. (2007) Supplemental evaluation of geophysical information used to detect and characterize buried volcanic features in the Yucca Mountain region. Technical Report NRC-02-02-012, Center for Nuclear Waste Regulatory Analyses, San Antonio, Texas. 12, 13

Stamatakos, J. A., Connor, C. B. & Martin, R. H. (1997) Quaternary basin evolution and basaltic volcanism of Crater Flat, Nevada, from detailed ground magnetic surveys of the Little Cones. *The Journal of Geology*, **105**(3):319–330. 2, 4, 12, 13

Thompson, G. (2000) Chapter E: Perspectives on Basin and Range structure and basaltic volcanism – Bare Mountain – Crater Flat area, Nye County, Nevada. *In* J.W. Whitney & W.R. Keefer (eds.) *Geologic and Geophysical Characterization Studies of Yucca Mountain, Nevada, A Potential High-Level Radioactive-Waste Repository*, Digital Data Series 58. US Geological Survey. 4

USGS (2001) Six aeromagnetic surveys in Nevada and California. Open-File Report 01–145, United States Geological Survey. URL http://pubs.usgs.gov/of/2001/ofr-01-0145/html/nevcal.html. 2, 7, 11

Valentine, G. A. & Perry, F. V. (2006) Decreasing magmatic footprints of individual volcanoes in a waning basaltic field. *Geophysical Research Letters*, **33**(14):1–5. ISSN 1944-8007. doi:10.1029/2006GL026743. URL http://dx.doi.org/10.1029/2006GL026743. 12

Valentine, G. A. & Perry, F. V. (2009) Volcanic risk assessment at Yucca Mountain, Nevada, USA: Integration of geophysics, geology, and modeling. *In* C.B. Connor, N.A. Chapman & L.J. Connor (eds.) *Volcanic and Tectonic Hazard Assessment for Nuclear Facilities. Cambridge University Press, New York*, 452–480. Cambridge University Press, Cambridge, UK. 2

Valentine, G. A., Perry, F. V., Krier, D., Keating, G. N., Kelley, R. E. & Cogbill, A. H. (2006) Small-volume basaltic volcanoes: Eruptive products and processes, and posteruptive geomorphic evolution in Crater Flat (Pleistocene), southern Nevada. *Geological Society of America Bulletin*, **118**(11-12):1313–1330. 2

Wessel, P. & Smith, W. H. F. (1998) New, improved version of Generic Mapping Tools released. *Eos, Transactions of the American Geophysical Union*, **79**(47):579–579. 16

Wetmore, P. H., Hughes, S. S., Connor, L. J. & Caplinger, M. L. (2009) Spatial distribution of eruptive centers about the Idaho National Laboratory. *In* C.B. Connor, N.A. Chapman & L.J. Connor (eds.) *Volcanic and Tectonic Hazard Assessment for Nuclear Facilities*, 229–256. Cambridge University Press, Cambride, UK. 2

Additional Files

Additional files include *(i)* a compressed file (`survey2014.zip`) containing the unprocessed magnetic and GPS data files collected during the 2014 USF ground-based survey and the PERL scripts used for time-stamp-matching, data processing and preparation of the final 2014 data file, (ii) a metadata file, for the 2014 ground magnetic survey (`survey2014_metadata.pdf`), and *(iii)* the processed magnetic data used to make the contour map in Figure 3A (`all_AnomalyB.zip`), including magnetic readings from an earlier 2011 survey that have been processed the same as the 2014 data but not drift corrected. The following provides a description of these files.

1: `survey2014.zip` is a compressed file that extracts to a single top-level directory, `AnomalyB-2014survey`, which contains a number of PERL (`.pl`) files and the following directory structure:

`drift gpsDG100 mag858 scripts`

Within the top-level directory, there is a PERL (`.pl`) script for each day that data was collected; these filenames beginning with `run-`. These scripts start the processing of magnetic data collected during one day; their operation is described below. The unprocessed magnetic data are contained within the `mag858` directory. The data format of these files is the Geometrics 858 text format (`*.stn`) after *binary-to-text* conversion using the Magmap2000 software. Corresponding GPS data collected contemporaneously with the magnetic data are contained within the `gpsD100` directory. These 7-column text files (`*.csv`) are formatted as *comma-separated-values*; column headings are at the top of each file. Daily data directories are named as $MMDDYYYYx$, where MM is the month, DD is the day, $YYYY$ is the year and x is either a or b representing a pair of instruments operating on the same day (*e.g.,* 03292014a and 03292014b). This naming convention is found in both the `mag858` and `gpsD100` directories. The magnetic and GPS data files are also named using this $MMDDYYYYx$ system and include file extensions `.stn` and `.csv`, respectively.
Magnetic drift data recorded by the Boulder Magnetic Observatory are contained in the `drift` directory. These files are organized by day beginning 03/23/2014 and ending 04/02/2014. The file names follow the $MMDDYYYYx$ naming convention and include a file extension `.dft`.
PERL data processing scripts are located in the scripts directory; the function of each script is described below. In the top-level directory, master `run-MMDDYYYYx.pl` PERL scripts will process corresponding days of collected data. A shell script (`run_all.sh`) directs the complete data processing workflow.

2: `survey2014_metadata.pdf` is a metadata file for the 2014 ground magnetic survey following the FGDC Content Standards for Digital Geospatial Metadata, version FDGC-STD-001-1998.

3: `all_AnomalyB.zip` is a compressed file that extracts to `all_AnomalyB.wgs84z11.xyz`, a combined dataset of 2014 and 2011 survey data that has been processed and filtered to make the GMT (Generic Mapping Tools) contour map in Figure 3A. The data format of this text file is:
Northing(m) Easting(m) Processed(nT) Observed(nT)

PERL scripts for data processing

Data processing is accomplished using command line PERL scripts. PERL was chosen because of its ability to quickly and easily scan and process columns of data line-by-line; all operating systems include a PERL interpreter. Each of these processing scripts are short and perform a single function (these are detailed below). They are simple text files that can easily be modified to accommodate alternative instrumentation or output style.

1: `run_all.sh` is the master shell script that will process all of the 2014 survey data. To run this shell script type:

```
sh run_all.sh
```

The output is a text file named, `anomalyB-2014.wgs84z11.dat`. This file has 9 data columns each separated by a space:

East(m) North(m) MagFinal(nT) MagObs(nT) MagDC(nT) Drift(nT) Date(m/d/y) Time(hh:mm:ss) Time(h.h)

2: `run-MMDDYYYYx.pl` PERL script that executes a set of processing PERL scripts, once for each daily set of collected data (magnetic and GPS). The month-day-year of data collection is included in the file name. If multiple files are collected per day then these are identified by a lower case letter after the date. The inputs to this script are specified and edited at the top of the script file as explained below.

INPUT VARIABLES:

$date : $MMDDYYYYx$ name of the daily survey file being processed, *e.g.,* `03292014a`.

$gps_model : model name for the GPS receiver used to collect the data. Currently, these scripts are set up to handle a GlobalSat DG100 GPS receiver and data collector.

$gps_dir : directory name where the unprocessed GPS data can be found.

$mag_dir : directory name where the unprocessed magnetic data can be found.

$drift_dir : file name of data for the daily drift correction. This name should include the directory name with the filename, *e.g.,* `drift/03262014.dft`.

$hour : an offset time (in hours) to synchronize the start of data collection times between the GPS and the magnetometer. This value will be *added to* or *subtracted from* the magnetometer time (defaults to 0).

$utm_zone : UTM zone number of the area where the data were collected (Anomaly B is located in UTM zone 11).

$slope : a smoothing value ($\mathrm{nT\,m^{-1}}$) applied to the data to remove data spikes (a value of 75 was used for the 2014 survey).

$igrf : the International Geomagnetic Reference Field (IGRF) value for the survey area during the time of data collection (49083.5 is used for the 2014 survey). This value is subtracted from each data reading.

OUTPUTS: An output directory is created for each set of daily processed files (magnetic and associated GPS data). The name of the directory follows the $MMDDYYYYx$ format. A `run-*.pl` script calls each of the data processing PERL scripts in the `scripts` directory for a day of data. Processing is complete when the word *Done* is seen on the command line. After each individual processing script has completed its processing task an intermediate file is created before running the next script in the sequence. Each subsequent script performs its function on the newly saved intermediate file created during the previous step. The final product is a file containing the drift corrected, time-matched, despiked, IGRF removed anomalous magnetic data file for one day of processed survey data, named `match_$MMDDYYYYx$.xyz.utm.F`. Intermediate files are retained in the output directory.

3: `dg100_to_decimal_time_decimal_deg.pl` PERL script that converts the GlobalSat DG100-GPS time and location data to decimal hours and decimal degrees, respectively.

INPUT PARAMETERS: name of the data file saved from the DG100 GPS receiver that has been converted to *csv* (comma separated values) format (specified after the script name on the command line).

OUTPUTS: 4 data columns in the following format:

Time(h.h) Latitude(d.d) Longitude(d.d) Time(original)

4: `stn2decimal_time.pl` PERL script that parses and converts the Geometrics mag858 text file to a column format and converts the time data to decimal hours.
INPUT PARAMETERS: name of the data file from the 858 Geometrics magnetometer that has been converted from binary to text format (specified after the script name on the command line)
OUTPUTS: 4 data columns in the following format:
Time(h.h) Mag(nT) Time(original) Date(original)

5: `reverse.pl` PERL script that reverses the sorted order of magnetic data with respect to time, from ascending to descending time to match the descending order of the GPS data file.
INPUT PARAMETERS: name of a data file (specified after the script name on the command line)
OUTPUTS: each input line of data, but in reversed order (last in, first out order)

6: `drift.pl` PERL script that corrects each magnetic reading for instrument drift using a data file of quality controlled magnetic readings of Earth's magnetic field recorded at a single location at a 1 minute frequency.
INPUT PARAMETERS: *(i)* name of a data file of magnetic readings, column formatted as specified in the output of item 4, *(ii)* name of a data file of drift values, column formatted as:
Date(dd/mm/yyyy) Time(hh:mm:ss) Drift(nT)
OUTPUTS: 6 data columns in the following format:
MagTime(h.h) MagDC(nT) MagObs(nT) Drift(nT) Time(hh:mm:s.s) Date(mm/dd/yyyy)

7: `match_mag_gps.pl` PERL script that combines the magnetic readings with the GPS locations by time-stamp-matching and collating the data from both files (858-mag and DG100-GPS) into a single output. Not matched magnetic readings are written to a *log* file in the top-level directory.
INPUT PARAMETERS: *(i)* name of a data file of magnetic readings, processed and column formatted as specified in the output of item 4, *(ii)* name of a data file of GPS readings, processed and column formatted as specified in the output of item 5
OUTPUTS: 8 columns of data in the following format:
Long(d.d) Lat(d.d) MagObs(nT) MagDC(nT) Drift(nT) Date(mm/dd/yyyy) Time(hh:mm:s.s) Time()h.h

8: `lonlat2utm.pl` PERL script that converts longitude and latitude locations (degrees) to UTM (meters) using the PROJ.4 - Cartographic Projections Library (*PROJ.4 Development Team*, 2014).
INPUT PARAMETERS: *(i)* name of a data file of located magnetic readings with the longitude and latitude in the first 2 columns, *(i)* UTM zone number for the survey location
OUTPUTS: same data format as the input file but the first 2 columns will be the easting and northing in meters

9: `filter_mag.pl` PERL script that smooths the magnetic data by removing dropouts (zero values) and data spikes (out-of-range high and low values) using a slope filtering algorithm between neighboring data points. Data spikes are removed based on the magnetic gradient. If the magnetic gradient exceeds the specified input value ($\$slope$; $\mathrm{nT\,m^{-1}}$) then this data point is considered to be out-of-range and is deleted. The IGRF correction is also performed during this step. At this point the magnetic values should range between a positive and negative value centered approximately at zero.
INPUT PARAMETERS: *(i)* filename of magnetic data, *(ii)* slope value in nT, *(iii)* IGRF value for survey area
OUTPUTS: 9 columns of data in the following format:
East(m) North(m) MagFinal(nT) MagObs(nT) MagDC(nT) Drift(nT) Date(mm/dd/yyyy) Time(hh:mm:s.s) Time(h.h)

These PERL scripts are executed from the command line:
`perl <script name>.pl <inputfile> <input parameters> > <outputfile>`
Input parameters are specified after the script name. The output can be redirected to a file using the UNIX redirection symbol > and an output filename.

Two additional scripts are provided in this folder: *histogram.pl* and *plot_points.gmt.pl*. These scripts provide a quick visualization of the processed data collected during that day. However, they require the installation of GMT version 5. Their execution has been disabled in the `run-MMDDYYYYx.pl` scripts.

Workflow for processing the 2014 survey data

The file `survey2014.zip` contains a complete listing of all unprocessed files and programs. The following workflow will explain how to reprocess the data and provides an example for processing future magnetic surveys in a similar fashion.

Step 1: Download and unzip the file `survey2014.zip`. This will set up the directory structure necessary for data processing, as described previously. All magnetic, GPS, and drift files have been placed in the appropriate directories. Additional surveys should follow this directory and file location structure.

Step 2: Edit file and directory names to reflect the date of data collection; this has already been done for the included 2014 survey data.

Step 3: Edit the parameters at the top of the `run-MMDDYYYYx.pl` script file for each day of collected data; this has already been done for the included 2014 survey files. The `run-MMDDYYYYx.pl` file must be located in the top level directory with the `drift`, `gpsDG100`, `mag858`, and `scripts` directories. As described previously, the `run_all.sh` shell script is written to process all data files from a single script. Each of the commands in this script can be run individually. This is the case during data collection; each daily set of data files are processed after collection. The master shell script is just provided for convenience.

Step 4: Execute the `run_all.sh` shell script or each `run-MMDDYYYYx.pl` PERL script:
`sh run_all.sh` or `perl run-MMDDYYYYx.pl` Now, output directories will be created and the intermediate and processed data files will be placed in their corresponding directory; the output directory will have the same name as the day file being processed. The intermediate data files will follow this specific naming convention:

`MMDDYYYYx.csv.D` has been processed by the *dg100_to_decimal_time_decimal_deg.pl* PERL script.

`MMDDYYYYx.stn.D` has been processed by the *stn2decimal_time.pl* PERL script.

`MMDDYYYYx.stn.D.r` has been processed by the *stn2decimal_time.pl, reverse.pl* PERL scripts.

`MMDDYYYYx.stn.D.r.dc` has been processed by the *stn2decimal_time.pl, reverse.pl, drift.pl* PERL scripts.

`match_MMDDYYYYx.xyz` has been processed by the *dg100_to_decimal_time_decimal_deg.pl, stn2decimal_time.pl, reverse.pl, drift.pl, match_mag_gps.pl* PERL scripts.

`match_MMDDYYYYx.xyz.utm` has been processed by the *dg100_to_decimal_time_decimal_deg.pl, stn2decimal_time.pl, reverse.pl, drift.pl, match_mag_gps.pl, lonlat2utm.pl* PERL scripts.

`match_MMDDYYYYx.xyz.utm.F` has been processed by the *dg100_to_decimal_time_decimal_deg.pl, stn2decimal_time.pl, reverse.pl, drift.pl, match_mag_gps.pl, lonlat2utm.pl, filter_mag.pl* PERL scripts.

After all processing steps have been completed, each processed daily file will be named `match_MMDDYYYY.xyz.utm.F`. Each processed `match_MMDDYYYY.xyz.utm.F` daily file can be concatenated into a single file with the UNIX command, `cat` ; this final concatenation step is completed in the `run_all.sh` shell script. For the 2014 survey, the final processed data file is named, `USF-anomalyB-2014.wgs84z11.dat` and will be located in the top-level directory.

Should processing be attempted more than once, please delete the output directories before re-running the workflow scripts.